Published in final edited form as:
Sci Transl Med. 2013 May 29; 5(187): . doi:10.1126/scitranslmed.3005066.

Coronary microvascular pericytes are the cellular target of sunitinib malate induced cardiotoxicity

Vishnu Chintalgattu[1], **Meredith L. Rees**[2], **James C. Culver**[5], **Aditya Goel**[1], **Tilahu Jiffar**[7], **Jianhu Zhang**[8], **Kenneth Dunner Jr**[8], **Shibani Pati**[3], **James A. Bankson**[9], **Renata Pasqualini**[10], **Wadih Arap**[10], **Nathan S. Bryan**[4], **Heinrich Taegtmeyer**[2], **Robert R. Langley**[8], **Hui Yao**[11], **Michael E. Kupferman**[7], **Mark L. Entman**[6], **Mary E. Dickinson**[5], and **Aarif Y. Khakoo**[1]

[1]Amgen, Inc., Research, Metabolic Disorders, South San Francisco, CA

[2]Department of Medicine, University of Texas at Houston Medical School, Houston, TX

[3]Department of Surgery, University of Texas at Houston Medical School, Houston, TX

[4]Department of Integrative Biology and Pharmacology, University of Texas at Houston Medical School, Houston, TX

[5]Department of Molecular Physiology and Biophysics, Baylor College of Medicine, Houston, TX

[6]Department of Medicine, Baylor College of Medicine, Houston, TX

[7]Department of Head and Neck Surgery, University of Texas M.D. Anderson Cancer Center, Houston, TX

[8]Department of Cancer Biology, University of Texas M.D. Anderson Cancer Center, Houston, TX

[9]Department of Imaging Physics, University of Texas M.D. Anderson Cancer Center, Houston, TX

[10]David H. Koch Center and Department of Genitourinary Medical Oncology, University of Texas M.D. Anderson Cancer Center, Houston, TX

[11]Department of Bioinformatics and Computational Biology, University of Texas M.D. Anderson Cancer Center, Houston, TX

Abstract

Sunitinib malate is a multi-targeted receptor tyrosine kinase inhibitor used in the treatment of human malignancies. A substantial number of sunitinib-treated patients develop cardiac dysfunction, but the mechanism of sunitinib-induced cardiotoxicity is poorly understood. We show that mice treated with sunitinib develop cardiac and coronary microvascular dysfunction and exhibit an impaired cardiac response to stress. The physiological changes caused by treatment with sunitinib are accompanied by a substantial depletion of coronary microvascular pericytes. Pericytes are a cell type that is dependent on intact PDGFR signaling but whose role in the heart is poorly defined. Sunitinib-induced pericyte depletion and coronary microvascular dysfunction are

Correspondence should be addressed to: Aarif Y. Khakoo (akhakoo@amgen.com) or Vishnu Chintalgattu (vishnuc@amgen.com).

Author Contributions: AYK obtained the funding; VC, MLR, SP, RP, WA, NSB, MLE, MED, and AYK designed all experiments; VC, MLR, NSB, and AG performed in vitro and in vivo cardiovascular physiology studies; VC, JCC, JZ, KD, RRL performed tissue staining and analysis; JCC and MED developed, implemented, and analyzed studies of microvascular structure and function; HY assisted with analysis of gene expression microarray data; VC, MLR, TJ, and MEK executed and analyzed tumor xenograft studies; JAB designed and assisted with implementation of cardiac MR protocols; VC and AYK drafted the initial manuscript; MLR, JCC, SP JAB, RP, WA, NSB, HT, RRL, MEK, MLE, HY and MED provided feedback for revision of critical content of the manuscript.

Competing Interests: VC, AG, and AYK are fulltime employees of Amgen, Inc.

recapitulated by CP-673451, a structurally distinct PDGFR inhibitor, confirming the role of PDGFR in pericyte survival. Thalidomide, an anti-cancer agent that is known to exert beneficial effects on pericyte survival and function, prevents sunitinib-induced pericyte cell death *in vitro* and prevents sunitinib-induced cardiotoxicity *in vivo* in a mouse model. Our findings suggest that pericytes are the primary cellular target of sunitinib-induced cardiotoxicity and reveal the pericyte as a cell type of concern in the regulation of coronary microvascular function. Furthermore, our data provide preliminary evidence that thalidomide may prevent cardiotoxicity in sunitinib-treated cancer patients.

Introduction

Sunitinib malate (Pfizer) is a small-molecule inhibitor of multiple receptor tyrosine kinases. The primary targets of sunitinib include PDGF receptors (PDGFR-β and α), VEGF receptors (VEGFR-I, II, III), and stem cell factor receptor. Sunitinib is FDA-approved for the treatment of metastatic renal cell carcinoma, imatinib-resistant gastrointestinal stromal tumor and pancreatic neuroendocrine tumors.

Unfortunately, multiple studies indicate that a sizeable subset of sunitinib-treated patients develop left ventricular (LV) dysfunction and overt heart failure (1–6). The reported incidence of LV dysfunction due to sunitinib ranges from 4–28%. However, despite evidence of cardiac dysfunction as a toxicity of sunitinib therapy, the underlying mechanism of cardiotoxicity due to sunitinib remains unclear.

Understanding the molecular and cellular basis of cardiac toxicity due to targeted cancer therapies such as sunitinib is essential for developing safer and more effective therapeutics. In this study, we used a mouse model to show that cardiotoxicity due to sunitinib is attributable to a profound effect on coronary microvascular pericytes, resulting in coronary microvascular dysfunction, LV dysfunction, and an impaired response to cardiac stress. Our study also implicates PDGFR as the relevant target of sunitinib leading to cardiac toxicity, in line with the known role of PDGFR signaling in promoting pericyte growth and survival in development and in adult life(7–9). Importantly, sorafenib, another anti-cancer agent that targets PDGFR, has also been associated with drug-induced cardiac toxicity(2, 10) Finally, we show that thalidomide, an agent used in the treatment of multiple human malignancies, can prevent cardiac pericyte depletion and cardiac dysfunction due to sunitinib without affecting the anti-tumor effect of sunitinib.

Results

Sunitinib treatment induces cardiac dysfunction and coronary microvascular dysfunction

To determine the effects of sunitinib on cardiac and coronary function, we treated C57Bl/6 mice with sunitinib at 40 mg/kg/day. This is the minimal dosage at which robust anti-tumor efficacy is observed across a range of murine xenograft models(11). Importantly, the halflife of sunitinib in normal human volunteers is approximately 25-fold higher than that in mice(12, 13). Thus, an oral dose of sunitinib of 40 mg/kg/day achieves drug exposures in mice that are approximately 2.5 fold higher than normal human volunteers dosed at 50 mg/day, the typical clinical dose. Since only a subset of sunitinib-treated cancer patients develop cardiac toxicity and since drug exposure can vary widely in cancer patients for a number of reasons, including the presence of renal insufficiency or drug-drug interactions(14), we deemed this to be a relevant exposure to study potential cardiac toxicities of sunitinib in a mouse model. Sunitinib or vehicle was administered for up to 21 days, mirroring the typical 3-week dosage cycle in sunitinib-treated cancer patients. Sunitinib-treated mice showed significant ($p<0.0001$ at day 21) decreases in left ventricular ejection fraction (EF) (Fig. 1A

&1B). Overt pathologic cardiac hypertrophy or pulmonary edema were not observed in sunitinib-treated mice (Fig. 1C), but an increase in myocyte cross-sectional area (Fig. S1A) was observed, suggestive of mild cardiac hypertrophy.

Although sunitinib is associated with hypertension in subsets of patients(4), we did not observe elevations of blood pressure that might contribute to cardiac dysfunction. (Figs. 1D & S1B). However, vascular toxicity of sunitinib manifested in impaired coronary microvascular function. Measurement of coronary flow reserve (CFR) as an index of coronary microvascular function is a technique we have previously reported(15). Sunitinib-treated mice showed a marked decrease in CFR (Figs. 1E & 1F). Coronary microvascular dysfunction in sunitinib-treated mice was also demonstrated by measuring adenosine-induced coronary vasodilation in vivo (Fig. S1C) and ex vivo in hearts from sunitinib-treated mice (Fig. 1G). Comparing hearts from sunitinib-treated mice with controls, we observed no difference in coronary microvascular density (Fig. S1D), indicating that microvascular rarefaction was not responsible for sunitinib-induced coronary microvascular dysfunction.

To gain insight into sunitinib-induced contractile dysfunction, we performed gene expression microarrays on hearts from mice treated with sunitinib or vehicle for 3 or 7 days. Using a false discovery rate of 10%, we identified 65 genes that were upregulated in sunitinib-treated hearts compared with vehicle control at either day 3 or day 7. Intriguingly, of the 51 genes in this group with an annotated function, 14 such genes have been reported in the literature as being upregulated in conditions of hypoxia (Fig. S1E). Most notable amongst these is PHD3 (aka EGLN3), a prolyl 4-hydroxylase protein whose expression is exquisitely sensitive to hypoxia(16, 17), and which is upregulated in the heart in models of myocardial ischemia(18, 19) Quantitative RT-PCR demonstrated a robust upregulation of PHD3 in the hearts of sunitinib-treated mice at 3 and 7 days after treatment compared with vehicle control (Fig. 1H). These findings suggest that myocardial hypoxia may provide a mechanistic link between microvascular dysfunction and cardiac contractility defects due to sunitinib.

Sunitinib augments pressure overload-induced coronary and cardiac dysfunction

Because coronary microvascular dysfunction has been linked to the development of pathologic cardiac hypertrophy and heart failure in response to pressure overload(20), we hypothesized that sunitinib would impair the cardiac response to stress. In support of this hypothesis, we found that sunitinib-treated mice exhibited a reduction in cardiac-contractile reserve (Fig. 2A). To further explore the effects of sunitinib on the cardiac response to stress, we used transverse aortic constriction (TAC). 14 days after TAC, sunitinib-treated mice did not exhibit excess cardiac hypertrophy or pulmonary edema (Fig. 2B). However, sunitinib-treated mice exposed to TAC exhibited a reduction in cardiac function compared with vehicle-treated mice (Fig. 2C). In addition, sunitinib-treated mice exposed to TAC developed reductions in CFR relative to controls (Fig. 2D). The rise in coronary microvessel density in response to TAC was blunted in sunitinib-treated mice compared to vehicle-treated mice (Fig. 2E & 2F). In addition, sunitinib-treated mice developed enhanced cardiac fibrosis in response to TAC (Fig. 2G).

We interrogated the effects of sunitinib on one of its known targets, PDGFR, building on our prior work showing that TAC increases the expression and phosphorylation of PDGFR-β in the murine heart(15). We found that the TAC-induced increase in cardiac PDGFR-β phosphorylation was reduced in sunitinib-treated mice (Fig. 2H), however the ratio of phospho-total PDGFR-β levels in the heart was not significantly different in sunitinib-treated mice relative to controls after TAC (densitometric ratio 0.58 ± 0.2, sunitinib 14 day TAC; 0.47 ± 0.08, Vehicle 14 day TAC, n=4 per group, p=0.08). Instead, this finding was

driven by the unexpected lack of increase in total PDGFR-β in the heart in sunitinib-treated mice relative to controls 14 days after TAC.

Coronary microvascular dysfunction in sunitinib-treated mice is associated with loss of pericytes

We used acetylcholine, an endothelial-dependent coronary vasodilator, to study the cellular basis of sunitinib-induced coronary microvascular dysfunction in the absence of exogenous stress. Augmentation of coronary flow in response to acetylcholine in sunitinib-treated mice was substantially reduced in vivo (Fig. 3A) and ex vivo (Fig. S2A). To determine if endothelial dysfunction was the primary cause of sunitinib-induced coronary microvascular dysfunction, we used sodium nitroprusside (SNP), an endothelial-independent vasodilator. Hearts from sunitinib-treated mice demonstrated a substantial reduction in coronary flow across a broad range of SNP concentrations (Fig. 3B), suggesting that sunitinib produces coronary microvascular pathology independent of effects on the vascular endothelium.

Sunitinib is a PDGFR inhibitor, and both PDGF and PDGFR knockout mice develop vascular abnormalities during development due to defects in pericytes (8, 9). We therefore considered the possibility that sunitinib-induced coronary dysfunction could be due to drug-induced effects on coronary microvascular pericytes. In support of this hypothesis, we observed that PDGFR-β expression (a marker of pericytes (21)) was reduced in cardiac lysates from sunitinib-treated mice exposed to TAC (Fig. 2H) and in non-stressed sunitinib-treated mice (Fig. S2B). After 14 days of treatment with sunitinib, protein levels of the cell-surface proteoglycan NG2, another pericyte marker (22), were reduced in cardiac lysates from sunitinib-treated mice relative to controls (Fig. 3C). NG2 expression progressively decreased over time in the hearts of sunitinib-treated mice (Fig. 3D). With confocal microscopy, we observed that in vehicle-treated hearts (Fig. 3E, top panel), CD31 staining and NG2 staining were mostly co-localized, indicative of the intimate relation between the $NG2^+$ pericyte and the $CD31^+$ microvascular endothelium. However, in hearts from sunitinib-treated mice, staining with NG2 was dramatically reduced (Fig 3E, bottom panel; quantified in Fig. 3F); many $CD31^+$ microvessels therefore lacked colocalized pericytes. In addition to its utility as a pericyte marker, the proteoglycan NG2 is also expressed in some vascular smooth muscle (23). However, we observed no reduction in smoothmuscle actin co-staining in sunitinib-treated hearts compared with controls (Fig. S2C). Confocal microscopy of long-axis cardiac sections demonstrated the intimate relationship of $NG2^+$ pericytes and coronary microvessels in controls and a diminution of this relationship in hearts from sunitinib-treated mice (Fig. S2D).

That sunitinib-treated hearts lacked pericytes around microvessels was further shown by electron microscopy using a previously described method (24). Microvessels in vehicle-treated hearts were consistently overlaid with pericytes, whereas in sunitinib-treated hearts, we observed multiple microvessels that were largely uncovered with pericytes. Representative electron micrographs are shown in Fig. 3G and Fig. S2E. Because loss of pericytes in development (25) and in tumors (26) results in increased microvascular tortuosity, we asked whether there was a similar change in vascular morphology in hearts of sunitinib-treated mice. We observed an increase in coronary microvascular tortuosity in hearts from sunitinib-treated mice, shown visually in Fig. 3H. Quantification of vascular tortuosity indices revealed a significant increase in microvascular tortuosity in hearts from mice treated with sunitinib relative to controls (vehicle 1.073 ± 0.008; sunitinib 1.111 ± 0.004; $p = 0.0095$; two-sided Wilcoxon Rank Sum Test). We did not observe a significant increase in mean microvessel radius (vehicle 2.45 μM ± 0.18; sunitinib 2.61 μM ± 0.15; $p = 0.76$; two-sided Wilcoxon Rank Sum Test).

Loss of pericytes in other vascular beds has been demonstrated to increase vascular permeability (7). After infusing a fluorescent-tagged 0.9 kDa molecule, we observed increased interstitial extravasation of the tagged molecule in sunitinib-treated mice compared with controls, indicative of enhanced coronary microvascular permeability in sunitinib-treated mice (representative sections shown in Fig. S2F). Quantifying this signal in multiple sections from sunitinib-treated or vehicle-treated mice revealed a 2.3 fold increase in vascular permeability of the microvessels of sunitinib-treated mice compared with controls ($p < 0.05$), further demonstrating the phenotype of pericyte loss in the heart due to sunitinib.

Pericyte abnormalities are not observed in skeletal muscle in sunitinib-treated mice and are not observed in a doxorubicin model of cardiac toxicity

We asked if sunitinib caused injury to other vascular structures. The vasoconstrictor response to phenylephrine was indistinguishable between aortas from mice treated for 14 days with sunitinib or vehicle (Fig. 4A). Similarly, we observed no significant effect of sunitinib on acetylcholine-induced aortic vasodilatation (Fig. 4B). Whereas cardiac dysfunction has been reported in subsets of sunitinib-treated patients, skeletal muscle pathology (such as atrophy or weakness) is not associated with sunitinib treatment. In mice treated with sunitinib, Western blotting of skeletal muscle lysates revealed no consistent reduction in pericyte markers NG2 or PDGFR-β, in comparison to vehicle-treated mice (Fig S2G). Confocal microscopy confirmed that pericyte coverage of $CD31^+$ microvessels in skeletal muscle was not affected by treatment with sunitinib (shown visually in Fig 4C and quantified in Figs 4D).

To determine whether pericyte loss due to sunitinib was a non-specific response to cardiac injury, we treated mice with the known cardiotoxin doxorubicin. Mice exposed to doxorubicin demonstrated reductions in cardiac ejection fraction (Fig. 4E). Treatment with doxorubicin also induced coronary microvascular dysfunction (Fig. 4F). However, cardiac lysates from doxorubicin-treated mice exhibited no reduction in expression of the pericyte marker NG2 (Fig. 4G); furthermore, confocal micrographs demonstrating the colocalization of pericytes with coronary microvessels in doxorubicin-treated mice were indistinguishable from controls (Fig. 4H). Thus, the effects of sunitinib on coronary microvascular pericytes are not a non-specific response to drugs that induce cardiotoxicity.

Sunitinib-induced coronary microvascular dysfunction and pericyte loss is recapitulated by the PDGFR inhibitor CP-673451

To further determine the contribution of PDGFR inhibition to sunitinib-induced pericyte loss and coronary microvascular dysfunction, we used the compound CP-673451, a PDGFR inhibitor that is structurally unrelated to sunitinib (Fig. 5A); unlike sunitinib, it displays negligible anti-VEGFR activity at drug exposure levels that inhibit PDGFR signaling (27). Treatment with CP-673451 did not increase heart weight or lung weight (Fig. 5B). However, mice treated with this inhibitor exhibited a decrease in ejection fraction (Fig. 5C) and coronary flow reserve (Fig. 5D), similar to the effect seen in mice treated with sunitinib. Confocal microscopy demonstrated reduction of pericyte coverage in coronary microvessels (Fig. 5E). Biochemical analysis of cardiac lysates from CP-673451 treated mice showed a decrease in expression of PDGFR-β, along with a clear reduction of the pericyte marker NG2 (shown in Fig. 5F, and quantified in Fig. 5G and 5H). These data, coupled with findings in sunitinib-treated mice, suggest that PDGFR inhibition underlies the development of cardiac and coronary microvascular toxicity due to sunitinib.

Sunitinib-induced cytotoxicity on coronary microvascular pericytes is ameliorated by cotreatment with thalidomide in vitro and in vivo

We measured the direct effects of sunitinib on pericytes in vitro. Sunitinib caused a dose dependent impairment of viability of pericytes (Fig. 6A). Because sunitinib-induced cardiotoxicity appears to be a result of direct effects on coronary pericytes, we reasoned that preventing sunitinib-induced pericyte loss could prevent cardiotoxicity due to sunitinib. Recent work suggested that the small-molecule therapeutic thalidomide can enhance pericyte proliferation, recruitment, and branching in vitro and promote pericyte coverage of immature vascular networks in vivo via pathways that partially depend on PDGFR signaling (28). These findings were consistent with prior studies demonstrating that tumors from mice treated with small-molecule thalidomide analogs have a two-fold increase in the number of pericyte-covered microvessels (29). These studies suggested that thalidomide could be an important tool to causally relate sunitinib cardiac toxicity to effects of the drug on pericytes. We found that thalidomide ameliorated the effects of sunitinib on in vitro pericyte proliferation, as measured by MTT assay (Fig. 6B) and real-time in vitro proliferation measurements (Fig. S3A). We did not observe an effect of sunitinib or thalidomide on primary fibroblast or endothelial cell viability in vitro (Figs. S3B & S3C). Thus, it appears that pericytes are most sensitive to the in vitro cytotoxicity of sunitinib and are also specifically protected by thalidomide. To determine if thalidomide can prevent sunitinib-induced cardiotoxicity in vivo, we co-administered thalidomide with sunitinib to C57BL/6 mice for 14 days, then stopped both agents and continued to assess the mice for 14 additional days (experimental schematic shown in Fig. 6C). Thalidomide exerted a protective effect on coronary microvascular dysfunction due to sunitinib in both the treatment and recovery phases of the protocol (Fig. 6D). Furthermore, co-administration of thalidomide prevented cardiac dysfunction due to sunitinib throughout the co-treatment period and into early recovery (Fig. 6E). Expression of the pericyte markers PDGFR-β and NG2 was greater in mice co-treated with sunitinib and thalidomide compared with sunitinib alone (Fig. 6F) at the end of the treatment phase, but expression of these markers was indistinguishable comparing the sunitinib and thalidomide-treated mice with mice that received sunitinib alone 14 days after recovery (Fig. 6F). Confocal microscopy showed preservation of pericyte coverage of coronary microvessels in mice treated with both thalidomide and sunitinib (Fig. 6G). These findings demonstrate a cardioprotective effect due to thalidomide and confirm the causal link between sunitinib-induced pericyte depletion and cardiac dysfunction due to sunitinib.

To ascertain whether the thalidomide rescue strategy might have clinical application, we studied the effects of co-administration of thalidomide and sunitinib in a human renal cell carcinoma xenograft model (30). Tumor volumes were measured bi-weekly until average tumor volume reached 250 mm^3. Mice were then divided into groups and treated with vehicle, thalidomide (75 μg/kg every other day; IP injection), sunitinib (40 mg/kg/d; oral gavage) or sunitinib + thalidomide for at least 28 days. Cardiac hypertrophy and pulmonary edema were not observed in any group (Fig. S3D). As observed in non-tumor bearing mice, co-treatment with thalidomide ameliorated the sunitinib-induced decline in cardiac function (Fig. S3E) and coronary microvascular function (Fig. S3F). Sunitinib robustly reduced the rate of tumor growth, and this effect was not significantly altered by co-administration of thalidomide (Fig. 6H); thalidomide itself exerted a minimal effect on the rate of tumor growth. Taken together, these findings suggest that co-administration of thalidomide may provide cardioprotection while preserving the anti-tumor effect in sunitinib-treated renal-cell carcinoma patients.

Discussion

We report here that the pericyte is the primary target of sunitinib-induced coronary microvascular abnormalities and cardiac dysfunction. Our findings to support this claim are 1) sunitinib-induced cardiotoxicity is associated with depletion of coronary microvascular pericytes resulting in changes in the coronary microvasculature; 2) pericyte loss is not a feature of doxorubicin-induced cardiotoxicity, and the effects of sunitinib on pericytes are specific to cardiac muscle; 3) pericyte loss and cardiac dysfunction seen with sunitinib is recapitulated by a structurally distinct inhibitor of PDGFR-β signaling, an essential pro-survival signaling pathway for pericytes; 4) the cytotoxic effect of sunitinib on pericytes is inhibited by thalidomide; and 5) thalidomide prevents cardiac toxicity and coronary microvascular dysfunction due to sunitinib in normal mice and in tumor-bearing mice.

Our study reports a physiological role for the pericyte as a regulator of coronary microvascular function in the adult, mammalian heart. Pericyte abnormalities have been correlated with cardiac developmental abnormalities in a variety of mouse lines (31, 32). Several additional reports have described the presence of pericytes in the adult rodent heart(24, 33), but the structural and functional descriptions of pericytes in these models were incompletely developed. In contrast, the functional role of vascular pericytes in the CNS has been appreciated for decades. A variety of critical functions have been ascribed to this cell type in the brain, including the maintenance of the blood-brain barrier and stabilization of cerebrovascular architecture(34). Lack of access to the CNS compartment may explain why sunitinib has not been reported to cause overt neurotoxicity due to effects on CNS pericytes in clinical studies or in pre-clinical models, including in our hands. Radiolabeling studies have demonstrated minimal accumulation of sunitinib in the central nervous system(13), perhaps due to the activity of the blood-brain barrier drug efflux transporters ABCB1 and ABCG2(35). Nonetheless, our findings suggest that a broad exploration of the effects of sunitinib on pericytes throughout the body is warranted.

Our findings indicate that pericytes are regulators of coronary microvascular function, but the precise mechanism by which pericytes impact coronary microvascular function remains undefined. Functional neuroimaging studies have demonstrated that cerebrovascular pericytes contract to maintain cerebrovascular blood flow (36). Pericytes can also produce specific growth factors (e.g. VEGF-A) that promote normal function and structure of the microvascular endothelium (37, 38). In addition, pericytes provide structural support of microvascular endothelial tubes by secreting specialized extracellular matrix (39). The contribution of each of these pericyte functions described in other organs to their role in the heart remains to be defined.

Another question is the cellular fate of pericytes in the hearts of sunitinib-treated mice. Although our in-vitro studies indicate a direct cytotoxic effect, these studies have insufficient temporal resolution to determine the true cellular fate of pericytes in vivo. Intriguingly, we observed that in mice treated with sunitinib, cardiac and coronary microvascular dysfunction was entirely reversible after a 2-week period of drug withdrawal. In addition, our findings indicated that the pericytes themselves are restored after withdrawal of sunitinib therapy. The reversibility of this phenotype is consistent with clinical reversibility of sunitinib cardiotoxicity, as recently reported (40). The cellular pool that contributes to the restoration of coronary microvascular pericytes after recovery from sunitinib cardiac toxicity is an important area for future study.

The fact that sunitinib-induced cardiac dysfunction is rescued by an intervention that prevents pericyte loss implies that the two phenomena are interdependent. A broad array of genes associated with hypoxia, including the hypoxia sensing gene PHD3, are upregulated

in hearts from mice treated with sunitinib, which suggests the intriguing possibility that sunitinib-induced microvascular dysfunction causes myocardial hypoxia, leading to a hibernating contractile state. However, we regard this connection as hypothesis-generating, and it will be important in future studies to specifically understand the extent of hypoxia in the hearts of sunitinib-treated animals and the contribution of myocardial hypoxia to the contractile dysfunction that we observed.

In addition, it is possible that effects of sunitinib not related to pericytes may contribute to sunitinib-induced contractile dysfunction. It has been previously reported that sunitinib can bind to and inhibit AMP-activated kinase(41) (an “off-target” effect), and that overexpression of an activated mutant of AMPK ameliorates sunitinib-induced cardiomyocyte cytotoxicity(42). This effect should not be overlooked, and more detailed studies are needed to understand the contribution of myocardial AMPK to the cardiotoxic effects of sunitinib-induced pericyte loss that we describe in this study.

Our study provides insight into the cellular regulation of coronary microvascular function. It is possible that cardiac pericyte abnormalities may play a role in heart failure not associated with cancer therapy, such as in those cases in which microvascular function is abnormal. Confirmation of this finding would implicate the enhancement of coronary microvascular pericyte function as a therapeutic goal for the treatment of human heart failure.

More specifically, our findings indicate that the effects of sunitinib on coronary microvascular pericytes are a result of inhibition of PDGFR signaling. Multiple anti-cancer drugs targeting PDGFR have been associated with clinical cardiotoxicity (2, 43). It should be noted, however, that alternative mechanisms of sunitinib-induced cardiotoxicity have also been demonstrated (4, 42), and these biologic effects may contribute to the phenotype that we have observed here. Additional clinical studies are warranted to determine whether sunitinib-induced coronary microvascular dysfunction and pericyte loss occurs in humans, and if low-dose thalidomide represents a rational cardioprotection strategy for patients at high risk for cardiotoxicity due to sunitinib.

Materials and Methods

Animal models and drugs

UT MD Anderson Cancer Center IACUC approved all animal protocols. Sunitinib (Pfizer, 10 mg/ml) was dissolved in an oral gavage solution (PEG-300 (10%), Tween-80 (0.5%), water, 0.1N hydrochloric acid, pH adjusted to 3.7). CP673451 was prepared according to previously described methods (27) and mice were treated via oral gavage (CP673451; 40 ng/kg/day) for 7–14 days. Thalidomide (Sigma-Aldrich, 75 μg/kg every other day; IP) was dissolved in DMSO and mice were treated on alternate days for 14–28 days. Doxorubicin (Sigma-Aldrich, 5 or 10 mg/kg/week; 7 or 14 days) was dissolved in PBS and mice were treated intraperitoneally for 7 or 14 days. Transverse aortic constriction (TAC) surgeries were performed based on previously described protocols (23). The sham procedure was similar, except that the aorta was not ligated.

Cardiac Magnetic Resonance Imaging

Cardiac function in experimental mice was measured by MR scanning using a previously described method(15). MR scanning experiments were performed with a Bruker 7.05-T MR scanner (Biospin MRI). Multislice, multiframe short axis gradient sequences were used to quantify LV end-diastolic and systolic volumes.

Coronary Flow by Ex-vivo Langendorff

Total coronary flow was measured using a Langendorff (Harvard Apparatus) device as described previously(44). Briefly, mice were deeply anesthetized with isoflurane. Hearts were removed, the aorta cannulated and perfused at a constant pressure of 80 mmHg with a modified Krebs-Henseleit buffer (120 mM NaCl, 5.9 mM KCl, 25 mM NaHCO3, 1.2 mM MgCl2, 2.5 mM CaCl2, 0.5 mM EDTA, 16.7 mM glucose) equilibrated with 95% O2–5% CO2 at 37oC. Hearts were surrounded with a 37oC water-jacketed bath. After an equilibration period of 20–30 minutes, hearts were perfused with increasing concentrations (10^{-9} to 10^{-5} M) of sodium nitroprusside (SNP) or adenosine or acetylcholine (10^{-8} M). Perfusate was collected from the coronaries for the duration of one minute every five minutes. Coronary flow rate was calculated as microliter of perfusate per minute per mg of heart.

Ultrasound measurement of coronary flow reserve

Coronary flow reserve was measured as previously described(15). Ratios of peak velocities at low (1%) and high (2.5%) dose isoflurane were reported as coronary flow reserve.

Cardiac Contractile Reserve (dP/dt_{max})

For measurements of cardiac contractility, maximum developed pressure in the left ventricle over time (dP/dt_{max}) was invasively measured with increasing concentration (1 mg/kg/min, 3 mg/kg/min, & 5 mg/kg/min) of dobutamine. Mice were deeply anesthetized with isoflurane. A pressure-sensitive probe (1F; Millar) was carefully inserted into the left ventricle. After stabilization of heart rate and LV pressures, various concentrations of dobutamine were infused through the tail vein, and left ventricular pressure and heart rate were recorded.

Immunoblot and quantitative densitometry

Standard Western blot protocol was used to measure protein levels (23). Primary antibodies were directed at the following antigens: PDGFR-β (1:200 dilution), NG2 chondroitin sulfate proteoglycan (NG2) (1:200 dilution) (Cell Signaling Technology) and phospho–PDGFR-β - Tyr 1021 (1:500 dilution) (Santa Cruz Biotechnology). Protein bands were quantified via densitometry using Fluorchem 8900 imaging software (Alpha Innotech). Protein expression was normalized to GAPDH (antibody from Cell Signaling Technology).

Vessel tortuosity

Tortuosity measurements were made in a blinded fashion. Sunitinib and vehicle-treated hearts were infused with 70 kDa tetramethylrhodamine-labeled dextran (Invitrogen). Hearts were placed in a 1% agarose gel mold poured into a glass-bottom culture dish (MatTek), and a bore approximately the diameter of the heart was created with molding clay. Confocal z-stacks were acquired to obtain three-dimensional images of vessels at the apex. Images of vessels were reconstructed and analyzed with Imaris (Bitplane). Custom-made ImarisXT extensions were written in MATLAB (Mathworks) to calculate vessel tortuosity for each branch (tortuosity, T, is defined as $T = L/D$, where L is the total arc length along a vessel trace, and D is the total displacement between the beginning and end of the branch). The tortuosity of all the vessels in a given image was calculated for each sample.

Immunofluorescence and confocal microscopy

Sections were incubated overnight at 4°C in Anti-NG2 or alpha smooth muscle actin (aSMC) (Sigma) (1:200 dilution; Chemicon USA) and anti-CD31 (1:200 dilution; PharMingen) in blocking buffer. After treatment with fluorescent-labeled secondary antibody and DAPI (4′,6-diamidine-2-phenyl indole.2HCl), sections were imaged with an

LSM 510 META inverted confocal microscope (Zeiss). Image J software (NIH) was used to measure the NG2 and CD31 coverage area of each image. All NG2/CD31 stained coronary microvessels were included in the analysis. The ratio between NG2 and CD31 pixel counts was used to quantify pericyte coverage. For assessment of vascular permeability (leak), 21 day SM or vehicle-treated hearts were infused with 200 ml 0.9 kDa lysine-fixable cadaverine conjugated to Alexa Fluor-555 (Life Technologies, 5 mg/ml in saline) directly into the left ventricle. After 10 minutes, hearts were fixed in 10% formalin overnight and then embedded in OCT, then processed for confocal imaging. Image J software (NIH) was used to quantify fluorescence (Alexa Fluor-555) of each image.

Measurement of microvascular density

Microvascular density was quantified by counting the number of $CD31^+$ microvessels relative to the number of cardiomyocyte nuclei per section using a technique that we have previously reported(15).

Wire myography

Wire myography on aortic rings to assess vascular contractility and relaxation was performed as previously described(45).

Scanning electron microscopy

Cardiac tissue preparation for electron microscopy was performed using a previously described method (24). Representative scanning electron micrographs were selected for presentation by an investigator (K.D.) blinded to the treatment allocation. Pseudocoloring of EM images was performed with Adobe Photoshop CS2. Grayscale images were colorized with the “Hue/Saturation” function and the “History Brush” tool to color specific structures recognizable by eye.

In vivo tumor xenograft

A sunitinib-sensitive, human-derived renal cell carcinoma cell line (786-0) was obtained from Dr. Eric Jonasch (MD Anderson Cancer Center). 10^7 cells were suspended in 150 μl of PBS, mixed with an equal volume of Matrigel (BD Biosciences) and injected subcutaneously into the left flank of 8-week-old male nude mice. Mice were euthanized when tumor volume exceeded 1500 mm^3.

RNA isolation for quantitative RT-PCR and gene expression microarrays

Total RNA was isolated from heart tissues using Trizol (Invitrogen) reagent using the manufacturer’s recommended protocol. RNA integrity was confirmed using an Agilent 2100 Bioanalyzer (Agilent Technologies), with samples run against an RNA ladder of specified molecular weights (Eukaryote Total RNA Nano Series II, Agilent Technologies)

Gene expression microarrays

Mouse genome 430 2.0 array gene chips were purchased from Affymetrix and probed with RNA according to the manufacturer’s recommended protocol using a double in vitro transcription method. The data were then processed for analysis.

In Vitro Pericyte proliferation Studies

Human placental pericytes (Promocell,) were used as a model system for in vitro pericyte studies. Similarly, human umbilical vein endothelial cells (HUVEC, Genlantis) and human cardiac fibroblasts (HCF, Cell Systems Corporation) were used as model systems to study endothelial cell and fibroblast behavior in vitro. Cells plated at 5000 cells/well were cultured

in Pericyte Growth Medium, which is supplemented with serum and growth factors (Promocell). Cells were then serum and growth factor starved in Pericyte Basal Medium (Promocell) for 6 hrs and treated with 0.01–100 μM sunitinib for 24 hrs. Cell proliferation was measured by MTT assay (Vybrant MTT, Invitrogen). In some experiments serum/growth factor starved cells were treated with 1μM thalidomide or DMSO for 30 min followed by addition of 1μM sunitinib. Cell proliferation was measured in real-time by Xcelligence System (Roche Applied Sciences) or by MTT assay. Cell proliferation was measured with MTT assay post-treatment with thalidomide and sunitinib.

Statistical Analysis

Data are presented as the mean ± S.E.M. Means were compared for statistical significance with an unpaired, 2-tailed Student's t test unless otherwise noted. Changes between multiple groups were evaluated with ANOVA, and Tukey's test was used to evaluate differences between individual groups. Differentially expressed genes in microarrays were identified by the modified t-tests implemented in the R package(46). The Benjamini-Hochberg method was used to control false discovery rate(47).

Supplementary Material

Refer to Web version on PubMed Central for supplementary material.

Acknowledgments

The authors are grateful to Dr. Brad Wong for assistance with pharmacokinetic calculations.

Funding: This work was supported in part by a Howard Hughes Medical Institute Physician-Scientist Early Career Award (to A.Y. Khakoo), a Physician-Scientist Award from the University of Texas MD Anderson Cancer Center (to A.Y. Khakoo), a Michael and Marriet Cyrus Scholar Award (to A.Y. Khakoo), NIH (RO1-HL102341 to A.Y. Khakoo), a Cancer Center Support Grant (P30-CA016672), the Experimental Cancer Imaging Research Program (U24-CA126577), and NIH 5R01HL061483-11 (to HT).

References and Notes

1. Di Lorenzo G, Autorino R, Bruni G, Carteni G, Ricevuto E, Tudini M, Ficorella C, Romano C, Aieta M, Giordano A, Giuliano M, Gonnella A, De Nunzio C, Rizzo M, Montesarchio V, Ewer M, De Placido S. Cardiovascular toxicity following sunitinib therapy in metastatic renal cell carcinoma: a multicenter analysis. Annals of Oncology. Sep.2009 20:1535. [PubMed: 19474115]
2. Schmidinger M, Zielinski CC, Vogl UM, Bojic A, Bojic M, Schukro C, Ruhsam M, Hejna M, Schmidinger H. Cardiac toxicity of sunitinib and sorafenib in patients with metastatic renal cell carcinoma. Journal of clinical oncology : official journal of the American Society of Clinical Oncology. Nov 10.2008 26:5204. [PubMed: 18838713]
3. Khakoo AY, Kassiotis CM, Tannir N, Plana JC, Halushka M, Bickford C 2nd, Trent J, Champion JC, Durand JB, Lenihan DJ. Heart failure associated with sunitinib malate: a multitargeted receptor tyrosine kinase inhibitor. Cancer. Jun.2008 112:2500. [PubMed: 18386829]
4. Chu TF, Rupnick MA, Kerkela R, Dallabrida SM, Zurakowski D, Nguyen L, Woulfe K, Pravda E, Cassiola F, Desai J, George S, Morgan JA, Harris DM, Ismail NS, Chen JH, Schoen FJ, Van den Abbeele AD, Demetri GD, Force T, Chen MH. Cardiotoxicity associated with tyrosine kinase inhibitor sunitinib. Lancet. Dec 15.2007 370:2011. [PubMed: 18083403]
5. Richards CJ, Je Y, Schutz FA, Heng DY, Dallabrida SM, Moslehi JJ, Choueiri TK. Incidence and risk of congestive heart failure in patients with renal and nonrenal cell carcinoma treated with sunitinib. Journal of clinical oncology : official journal of the American Society of Clinical Oncology. Sep 1.2011 29:3450. [PubMed: 21810682]
6. Telli ML, Witteles RM, Fisher GA, Srinivas S. Cardiotoxicity associated with the cancer therapeutic agent sunitinib malate. Annals of Oncology. Sep.2008 19:1613. [PubMed: 18436521]

7. Armulik A, Genove G, Mae M, Nisancioglu MH, Wallgard E, Niaudet C, He L, Norlin J, Lindblom P, Strittmatter K, Johansson BR, Betsholtz C. Pericytes regulate the blood-brain barrier. Nature. Nov 25.2010 468:557. [PubMed: 20944627]
8. Hellstrom M, Kalen M, Lindahl P, Abramsson A, Betsholtz C. Role of PDGF-B and PDGFR-beta in recruitment of vascular smooth muscle cells and pericytes during embryonic blood vessel formation in the mouse. Development. Jun.1999 126:3047. [PubMed: 10375497]
9. Lindahl P, Johansson BR, Leveen P, Betsholtz C. Pericyte loss and microaneurysm formation in PDGF-B-deficient mice. Science. Jul 11.1997 277:242. [PubMed: 9211853]
10. Uraizee I, Cheng S, Moslehi J. Reversible cardiomyopathy associated with sunitinib and sorafenib. New England Journal of Medicine. Oct 27.2011 365:1649. [PubMed: 22030001]
11. Mendel DB, Laird AD, Xin X, Louie SG, Christensen JG, Li G, Schreck RE, Abrams TJ, Ngai TJ, Lee LB, Murray LJ, Carver J, Chan E, Moss KG, Haznedar JO, Sukbuntherng J, Blake RA, Sun L, Tang C, Miller T, Shirazian S, McMahon G, Cherrington JM. In vivo antitumor activity of SU11248, a novel tyrosine kinase inhibitor targeting vascular endothelial growth factor and platelet-derived growth factor receptors: determination of a pharmacokinetic/pharmacodynamic relationship. Clinical cancer research : an official journal of the American Association for Cancer Research. Jan.2003 9:327. [PubMed: 12538485]
12. Haznedar JO, Patyna S, Bello CL, Peng GW, Speed W, Yu X, Zhang Q, Sukbuntherng J, Sweeny DJ, Antonian L, Wu EY. Single-and multiple-dose disposition kinetics of sunitinib malate, a multitargeted receptor tyrosine kinase inhibitor: comparative plasma kinetics in non-clinical species. Cancer chemotherapy and pharmacology. Sep.2009 64:691. [PubMed: 19169880]
13. Speed B, Bu HZ, Pool WF, Peng GW, Wu EY, Patyna S, Bello C, Kang P. Pharmacokinetics, distribution, and metabolism of [14C]sunitinib in rats, monkeys, and humans. Drug metabolism and disposition: the biological fate of chemicals. Mar.2012 40:539. [PubMed: 22180047]
14. Goodman VL, Rock EP, Dagher R, Ramchandani RP, Abraham S, Gobburu JV, Booth BP, Verbois SL, Morse DE, Liang CY, Chidambaram N, Jiang JX, Tang S, Mahjoob K, Justice R, Pazdur R. Approval summary: sunitinib for the treatment of imatinib refractory or intolerant gastrointestinal stromal tumors and advanced renal cell carcinoma. Clinical cancer research : an official journal of the American Association for Cancer Research. Mar 1.2007 13:1367. [PubMed: 17332278]
15. Chintalgattu V, Ai D, Langley RR, Zhang J, Bankson JA, Shih TL, Reddy AK, Coombes KR, Daher IN, Pati S, Patel SS, Pocius JS, Taffet GE, Buja LM, Entman ML, Khakoo AY. Cardiomyocyte PDGFR-beta signaling is an essential component of the mouse cardiac response to load-induced stress. Journal of Clinical Investigation. Feb 1.2010 120:472. [PubMed: 20071776]
16. Stiehl DP, Wirthner R, Koditz J, Spielmann P, Camenisch G, Wenger RH. Increased prolyl 4-hydroxylase domain proteins compensate for decreased oxygen levels. Evidence for an autoregulatory oxygen-sensing system. The Journal of biological chemistry. Aug 18.2006 281:23482. [PubMed: 16790428]
17. Koditz J, Nesper J, Wottawa M, Stiehl DP, Camenisch G, Franke C, Myllyharju J, Wenger RH, Katschinski DM. Oxygen-dependent ATF-4 stability is mediated by the PHD3 oxygen sensor. Blood. Nov 15.2007 110:3610. [PubMed: 17684156]
18. Willam C, Maxwell PH, Nichols L, Lygate C, Tian YM, Bernhardt W, Wiesener M, Ratcliffe PJ, Eckardt KU, Pugh CW. HIF prolyl hydroxylases in the rat; organ distribution and changes in expression following hypoxia and coronary artery ligation. Journal of molecular and cellular cardiology. Jul.2006 41:68. [PubMed: 16765982]
19. May D, Gilon D, Djonov V, Itin A, Lazarus A, Gordon O, Rosenberger C, Keshet E. Transgenic system for conditional induction and rescue of chronic myocardial hibernation provides insights into genomic programs of hibernation. Proceedings of the National Academy of Sciences of the United States of America. Jan 8.2008 105:282. [PubMed: 18162550]
20. Sano M, Minamino T, Toko H, Miyauchi H, Orimo M, Qin Y, Akazawa H, Tateno K, Kayama Y, Harada M, Shimizu I, Asahara T, Hamada H, Tomita S, Molkentin JD, Zou Y, Komuro I. p53-induced inhibition of Hif-1 causes cardiac dysfunction during pressure overload. Nature. Mar 22.2007 446:444. [PubMed: 17334357]
21. Abramsson A, Berlin O, Papayan H, Paulin D, Shani M, Betsholtz C. Analysis of mural cell recruitment to tumor vessels. Circulation. Jan 1.2002 105:112. [PubMed: 11772885]

22. Ozerdem U, Stallcup WB. Pathological angiogenesis is reduced by targeting pericytes via the NG2 proteoglycan. Angiogenesis. 2004; 7:269. [PubMed: 15609081]
23. Ozerdem U, Grako KA, Dahlin-Huppe K, Monosov E, Stallcup WB. NG2 proteoglycan is expressed exclusively by mural cells during vascular morphogenesis. Developmental dynamics : an official publication of the American Association of Anatomists. Oct.2001 222:218. [PubMed: 11668599]
24. Higuchi K, Hashizume H, Aizawa Y, Ushiki T. Scanning electron microscopic studies of the vascular smooth muscle cells and pericytes in the rat heart. Archives of Histology and Cytology. May.2000 63:115. [PubMed: 10885448]
25. Gaengel K, Genove G, Armulik A, Betsholtz C. Endothelial-mural cell signaling in vascular development and angiogenesis. Arteriosclerosis, thrombosis, and vascular biology. May.2009 29:630.
26. Carmeliet P, Jain RK. Principles and mechanisms of vessel normalization for cancer and other angiogenic diseases. Nature reviewsDrug discovery. Jun.2011 10:417.
27. Roberts WG, Whalen PM, Soderstrom E, Moraski G, Lyssikatos JP, Wang HF, Cooper B, Baker DA, Savage D, Dalvie D, Atherton JA, Ralston S, Szewc R, Kath JC, Lin J, Soderstrom C, Tkalcevic G, Cohen BD, Pollack V, Barth W, Hungerford W, Ung E. Antiangiogenic and antitumor activity of a selective PDGFR tyrosine kinase inhibitor, CP-673,451. Cancer Research. Feb 1.2005 65:957. [PubMed: 15705896]
28. Lebrin F, Srun S, Raymond K, Martin S, van den Brink S, Freitas C, Breant C, Mathivet T, Larrivee B, Thomas JL, Arthur HM, Westermann CJ, Disch F, Mager JJ, Snijder RJ, Eichmann A, Mummery CL. Thalidomide stimulates vessel maturation and reduces epistaxis in individuals with hereditary hemorrhagic telangiectasia. Nature Medicine. Apr.2010 16:420.
29. Gee MS, Makonnen S, al-Kofahi K, Roysam B, Payvandi F, Man HW, Muller GW, Lee WM. Selective cytokine inhibitory drugs with enhanced antiangiogenic activity control tumor growth through vascular inhibition. Cancer Research. Dec 1.2003 63:8073. [PubMed: 14678955]
30. Bhatt RS, Wang X, Zhang L, Collins MP, Signoretti S, Alsop DC, Goldberg SN, Atkins MB, Mier JW. Renal cancer resistance to antiangiogenic therapy is delayed by restoration of angiostatic signaling. Molecular cancer therapeutics. Oct.2010 9:2793. [PubMed: 20699227]
31. Jeansson M, Gawlik A, Anderson G, Li C, Kerjaschki D, Henkelman M, Quaggin SE. Angiopoietin-1 is essential in mouse vasculature during development and in response to injury. The Journal of clinical investigation. Jun 1.2011 121:2278. [PubMed: 21606590]
32. Bjarnegard M, Enge M, Norlin J, Gustafsdottir S, Fredriksson S, Abramsson A, Takemoto M, Gustafsson E, Fassler R, Betsholtz C. Endothelium-specific ablation of PDGFB leads to pericyte loss and glomerular cardiac and placental abnormalities. Development. Apr.2004 131:1847. [PubMed: 15084468]
33. Marini M, Falcieri E, Margonato V, Trere D, Lapalombella R, di Tullio S, Marchionni C, Burattini S, Samaja M, Esposito F, Veicsteinas A. Partial persistence of exercise-induced myocardial angiogenesis following 4-week detraining in the rat. Histochemistry and cell biology. Apr.2008 129:479. [PubMed: 18172661]
34. Winkler EA, Bell RD, Zlokovic BV. Central nervous system pericytes in health and disease. Nature neuroscience. 2011; 14:1398.
35. Tang SC, Lagas JS, Lankheet NA, Poller B, Hillebrand MJ, Rosing H, Beijnen JH, Schinkel AH. Brain accumulation of sunitinib is restricted by P-glycoprotein (ABCB1) and breast cancer resistance protein (ABCG2) and can be enhanced by oral elacridar and sunitinib coadministration. *International journal of cancer* . Journal international du cancer. Jan 1.2012 130:223. [PubMed: 21351087]
36. Fernandez-Klett F, Offenhauser N, Dirnagl U, Priller J, Lindauer U. Pericytes in capillaries are contractile in vivo, but arterioles mediate functional hyperemia in the mouse brain. Proceedings of the National Academy of Sciences of the United States of America. Dec 21.2010 107:22290. [PubMed: 21135230]
37. Song S, Ewald AJ, Stallcup W, Werb Z, Bergers G. PDGFRbeta+ perivascular progenitor cells in tumours regulate pericyte differentiation and vascular survival. Nature cell biology. Sep.2005 7:870.

38. Bergers G, Song S, Meyer-Morse N, Bergsland E, Hanahan D. Benefits of targeting both pericytes and endothelial cells in the tumor vasculature with kinase inhibitors. The Journal of clinical investigation. May.2003 111:1287. [PubMed: 12727920]
39. Rivera LB, Bradshaw AD, Brekken RA. The regulatory function of SPARC in vascular biology. Cellular and molecular life sciences : CMLS. Oct.2011 68:3165. [PubMed: 21822645]
40. Uraizee I, Cheng S, Moslehi J. Reversible cardiomyopathy associated with sunitinib and sorafenib. The New England journal of medicine. Oct 27.2011 365:1649. [PubMed: 22030001]
41. Laderoute KR, Calaoagan JM, Madrid PB, Klon AE, Ehrlich PJ. SU11248 (sunitinib) directly inhibits the activity of mammalian 5'-AMP-activated protein kinase (AMPK). Cancer biology & therapy. Jul 1.2010 10:68. [PubMed: 20495370]
42. Kerkela R, Woulfe KC, Durand JB, Vagnozzi R, Kramer D, Chu TF, Beahm C, Chen MH, Force T. Sunitinib-induced cardiotoxicity is mediated by off-target inhibition of AMP-activated protein kinase. Clin Transl Sci. Feb.2009 2:15. [PubMed: 20376335]
43. Kerkela R, Grazette L, Yacobi R, Iliescu C, Patten R, Beahm C, Walters B, Shevtsov S, Pesant S, Clubb FJ, Rosenzweig A, Salomon RN, Van Etten RA, Alroy J, Durand JB, Force T. Cardiotoxicity of the cancer therapeutic agent imatinib mesylate. Nature Medicine. Aug.2006 12:908.
44. Morrison RR, Tan XL, Ledent C, Mustafa SJ, Hofmann PA. Targeted deletion of A2A adenosine receptors attenuates the protective effects of myocardial postconditioning. *American journal of physiology* . Heart and circulatory physiology. Oct.2007 293:H2523. [PubMed: 17675570]
45. Erez A, Nagamani SC, Shchelochkov OA, Premkumar MH, Campeau PM, Chen Y, Garg HK, Li L, Mian A, Bertin TK, Black JO, Zeng H, Tang Y, Reddy AK, Summar M, O'Brien WE, Harrison DG, Mitch WE, Marini JC, Aschner JL, Bryan NS, Lee B. Requirement of argininosuccinate lyase for systemic nitric oxide production. Nat Med. Dec.2011 17:1619. [PubMed: 22081021]
46. Sjogren A, Kristiansson E, Rudemo M, Nerman O. Weighted analysis of general microarray experiments. BMC bioinformatics. 2007; 8:387. [PubMed: 17937807]
47. Hochberg Y, Benjamini Y. More powerful procedures for multiple significance testing. Statistics in medicine. Jul.1990 9:811. [PubMed: 2218183]

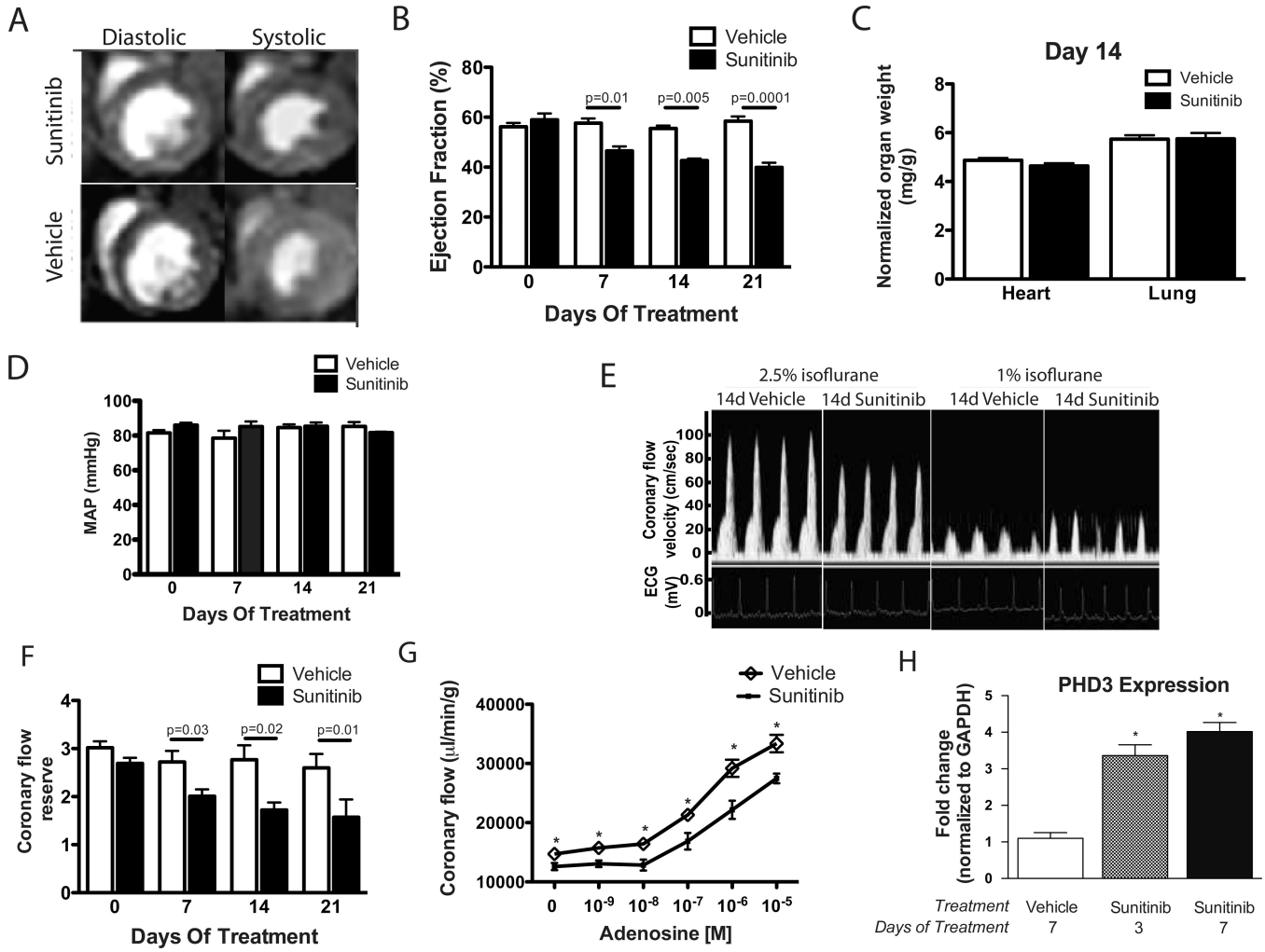

Fig. 1. Sunitinib treatment induces coronary microvascular dysfunction

(A) Representative cardiac MRI images from mice treated with sunitinib or vehicle for 14 days. (B) Left ventricular ejection fraction of treated mice at various time points (n= 7–10 mice per group). (C) Heart weight/body weight and lung weight/body weight ratios of mice treated for 14 days (n=7–10 mice per group). (D) Mean arterial pressure (MAP) in sunitinib or vehicle-exposed mice measured by tail cuff (n=5–6 mice per group). (E) Representative ultrasound tracings of dilated (induced with 2.5% isoflurane) and basal (with 1% isoflurane) coronary flow after 14 days of treatment. (F) Quantification of coronary flow reserve (dilated/basal flow) in sunitinib-treated and vehicle-treated mice (n=6–10 mice per group). (G) Total coronary flow in response to increasing concentrations of adenosine measured in ex-vivo heart preparations from sunitinib or vehicle-treated mice. (H) Quantitative RT-PCR results probing for PHD3 (normalized to GAPDH) using total RNA extracted from cardiac tissue of mice treated for the indicated number of days. * p <0.05

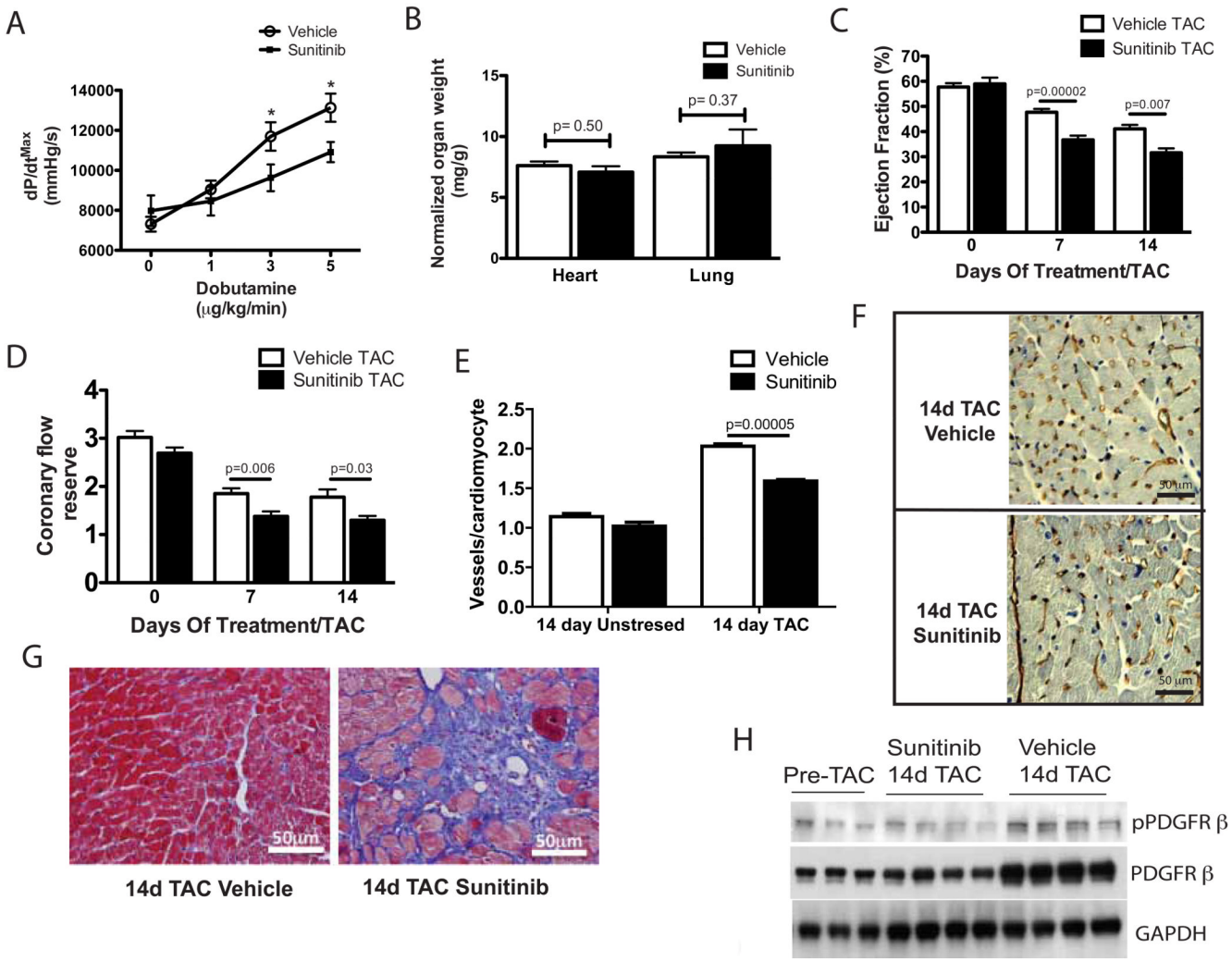

Fig. 2. Sunitinib augments pressure overload-induced cardiac dysfunction

(A) Cardiac contractile reserve (maximal developed pressure over time, dP/dt_{max}) in response to increasing concentrations of dobutamine in sunitinib or vehicle-treated mice (n=7–8). (B) Heart weight/body weight and lung weight/body weight ratios of sunitinib or vehicle-treated mice (n=8–9) after 14 days of TAC. (C) Cardiac ejection fraction in sunitinib or vehicle-treated mice as measured by cardiac MRI after 0, 7 and 14 days of TAC (n=9–10). (D) Coronary flow reserve in sunitinib or vehicle-treated mice after 0, 7, and 14 days of TAC (n=7–10). (E) Quantification of vessel densities ($CD31^+$ vessels/cardiomyocyte) in cardiac sections from sunitinib or vehicle-treated mice after 14 days of TAC or 14 days of treatment without TAC stress. (F) Immunohistochemical staining for CD31 in cardiac sections from sunitinib or vehicle-treated mice after 14 days of TAC. Scale bar = 50 μm. (G) Representative photomicrographs of Masson's trichrome stained cardiac sections from sunitinib or vehicle-treated mice after 14 days of TAC. Scale bar = 50 μm. (H) Phosphorylated and total PDGFR β protein in pre-TAC and 14-day TAC mice treated with sunitinib or vehicle. All results presented in this figure are representative of 2–3 independent experiments. * $p < 0.05$

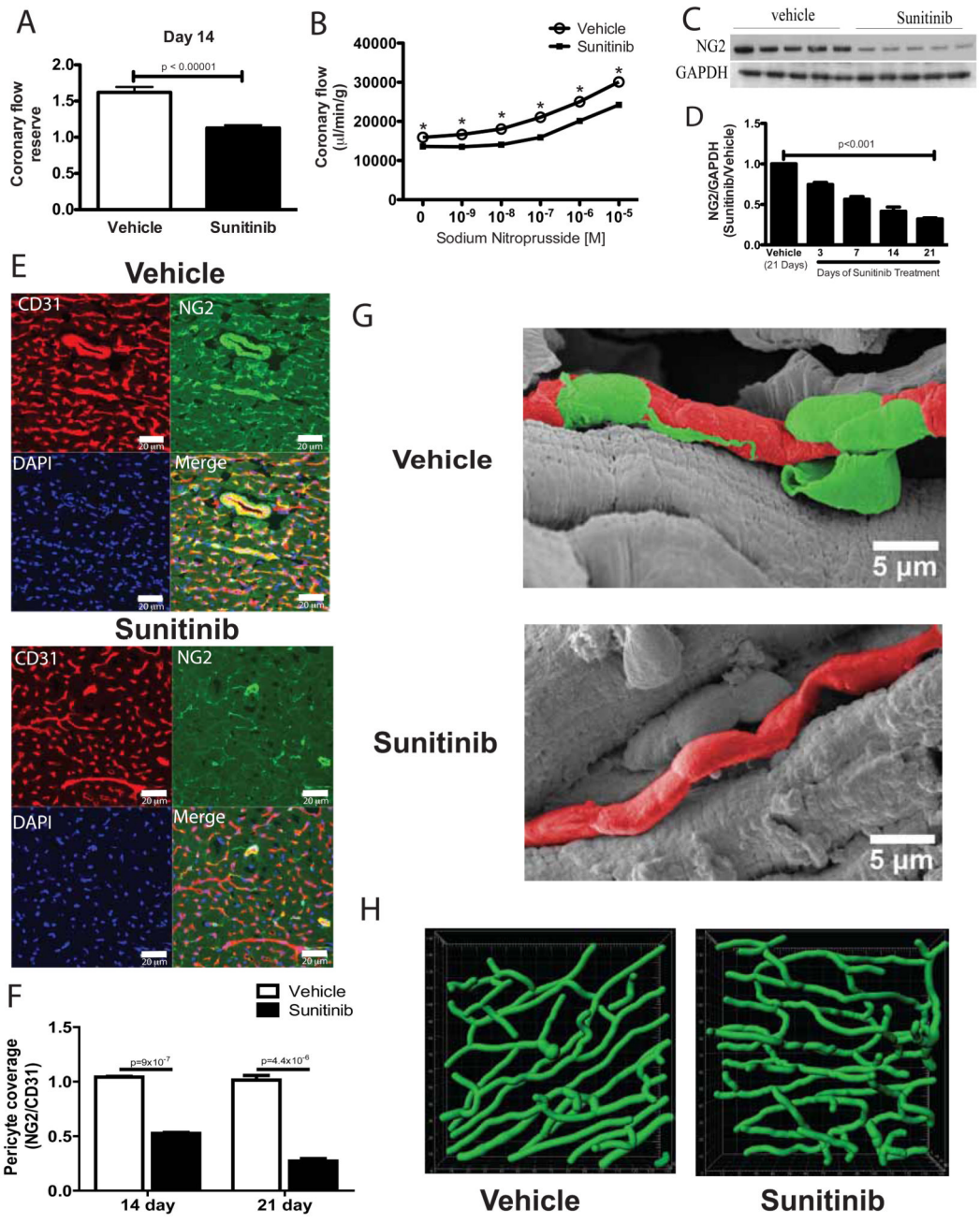

Fig. 3. Coronary microvascular dysfunction in sunitinib-treated mice is associated with loss of pericytes

(A) Coronary flow reserve in response to acetylcholine in mice treated for 14 days. (B) Total coronary flow in response to increasing concentrations of sodium nitroprusside measured ex vivo using hearts from sunitinib-treated or control mice after 14 days (n=7–8 hearts per group). (C) NG2 protein expression in cardiac lysates from mice treated for 14 days. (D) Densitometric quantification (from Western blotting) of NG2 protein normalized to GAPDH at 3, 7, 14, or 21 days in hearts from sunitinib-treated mice relative to controls (n=4–5 mice per time point); p-value calculated by ANOVA. (E) Confocal micrographs from representative cardiac sections showing staining for the endothelial cell marker CD31 (red),

the pericyte marker NG2 (green), nuclear staining with DAPI (blue) and the merged image (bottom right) from sunitinib (bottom panels) or vehicle-treated mice (top panels) after 14 days. Scale bar = 20 μm. (F) Quantification of $NG2^+$ pericyte coverage of $CD31^+$ microvessels in sunitinib or vehicle-treated mice after 14 or 21 days of treatment (n=4 animals per group). (G) Representative scanning electron micrographs of the cardiac microvasculature from control or sunitinib-treated mice after 14 days of treatment. Pseudocoloring is used (green for pericytes, red for microvessels) to aid in distinguishing pericytes from underlying microvessels; gray-scale electron micrographs are shown in Fig. S2E. Scale bar =5 μm. (H) Representative images of the coronary microvasculature derived from computer-based reconstruction of dextran-perfused hearts of sunitinib-treated mice (bottom panel) compared with vehicle-treated mice (top panel). * $p < 0.05$.

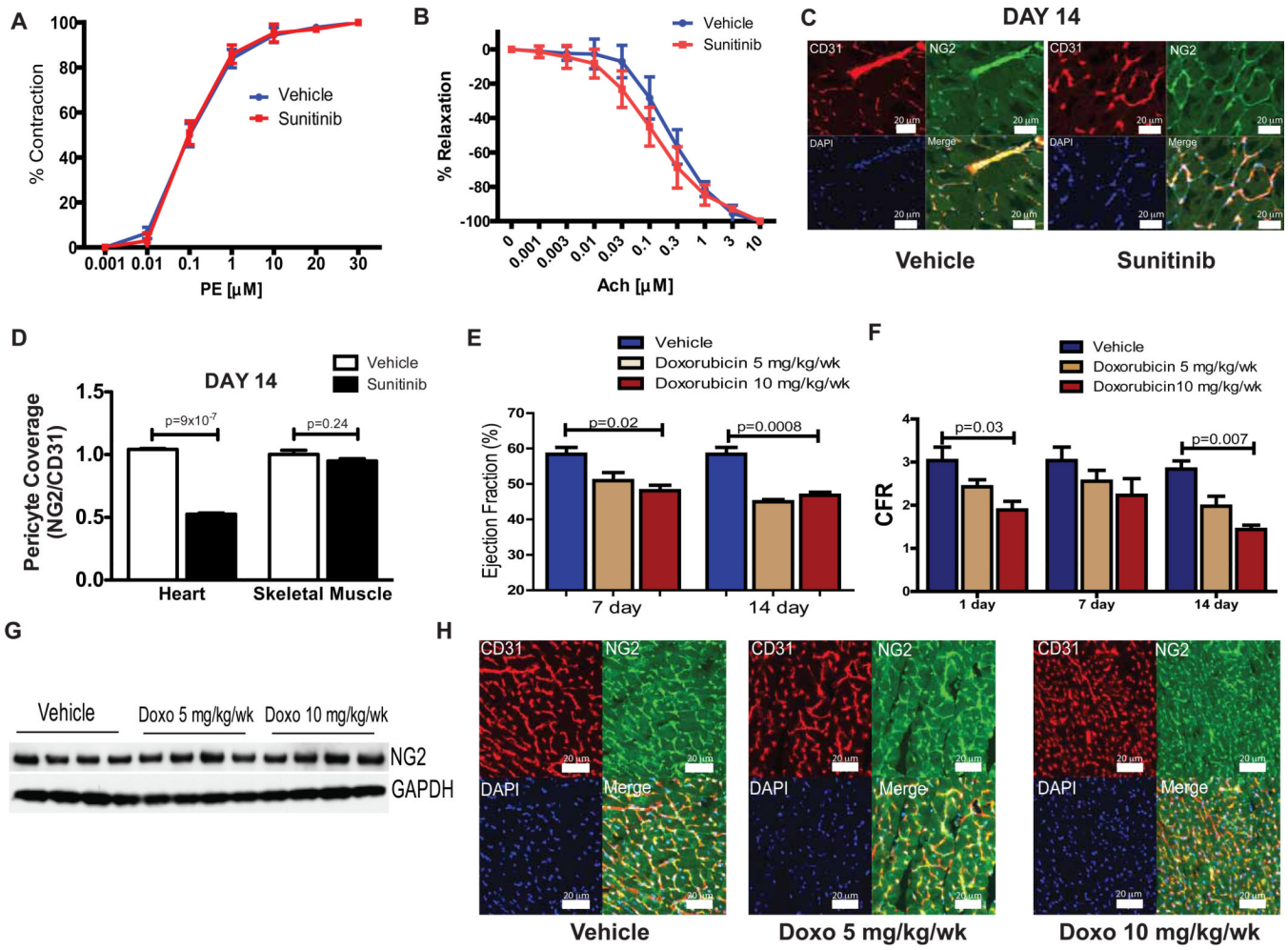

Fig. 4. Pericyte abnormalities are not observed in skeletal muscle or after doxorubicin treatment

Percent contraction or relaxation in the presence of (A) phenylephrine (PE) or (B) acetylcholine (Ach), respectively, in thoracic aortas isolated from mice treated with either sunitinib or vehicle (n=4–5). (C) Confocal micrographs from representative skeletal muscle (gastrocnemius) sections showing staining for the endothelial cell marker CD31 (red), the pericyte marker NG2 (green), nuclear staining with DAPI (blue) and the merged image (bottom right) from sunitinib (right panels) or vehicle-treated mice (left panels) after 14 days. Scale bar = 20 µm. (D) Quantification of coverage of $CD31^+$ microvessels by $NG2^+$ pericytes in heart and skeletal muscle isolated from treated mice (n=4 mice per group). (E) Cardiac ejection fraction in doxorubicin or vehicle-treated mice, as measured by cardiac MRI (n=4–5 mice per group). (F) Coronary flow reserve in doxorubicin or vehicle-treated mice (n=4–5 mice per group). (G) NG2 protein expression (by Western blot) in cardiac lysates from doxorubicin or vehicle-treated mice. (H) Confocal micrographs from representative cardiac sections showing staining for the endothelial cell marker CD31 (red), pericyte marker NG2 (green), nuclear stain for DAPI (blue) and the merged image (bottom right) from mice treated with vehicle control (left panels), 5 mg/kg/wk doxorubicin (center panels) or 10 mg/kg/wk doxorubicin (right panels). Scale bar = 20 µm. All results presented in this figure are representative of 2–3 independent experiments, * $p < 0.05$.

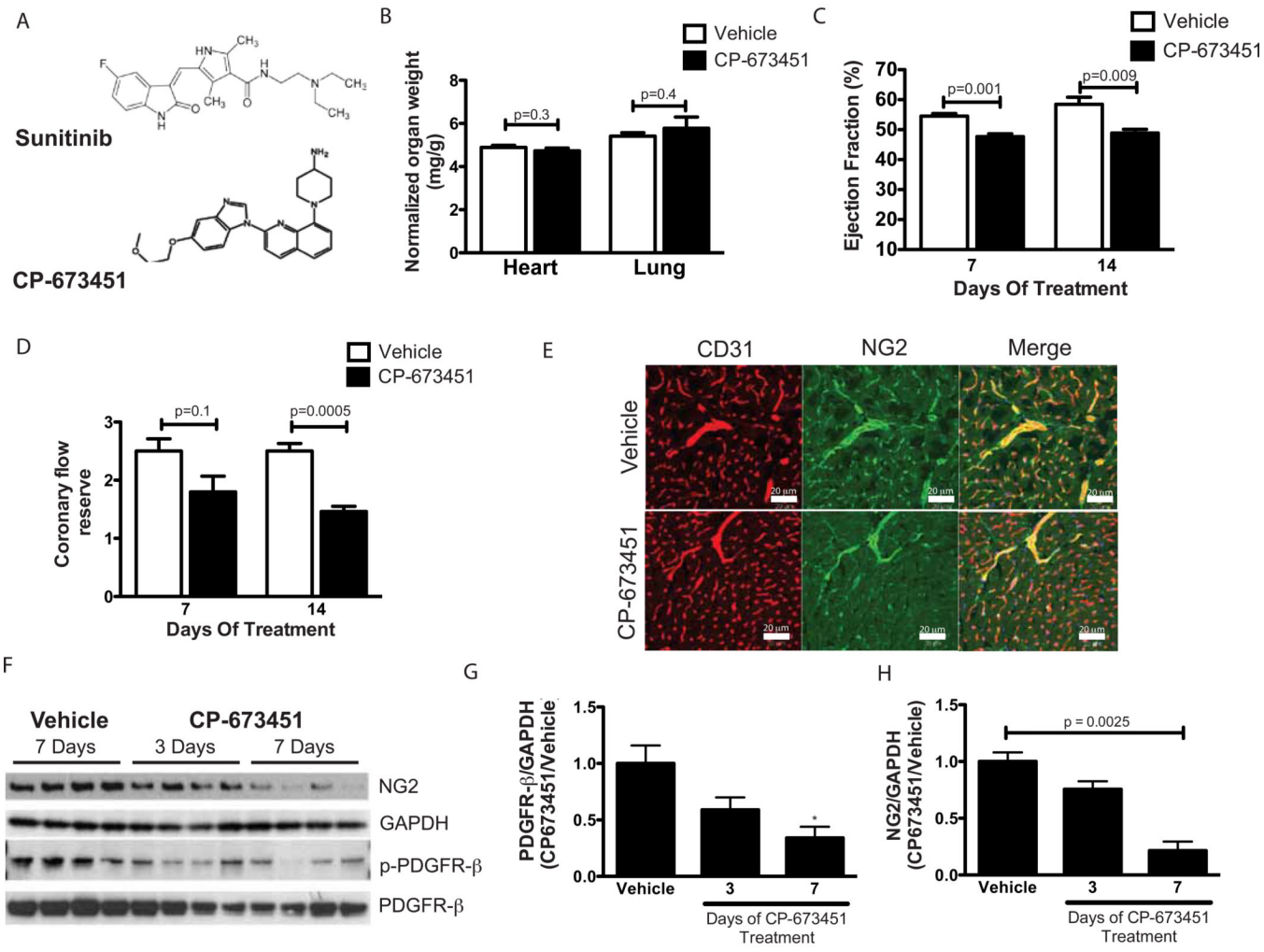

Fig. 5. Sunitinib-induced coronary dysfunction and pericyte loss is recapitulated by a PDGFR inhibitor

(A) Chemical structures of sunitinib and CP-673451. (B) Heart weight or lung weight to body weight ratios in CP-673451 or vehicle-treated mice (n=5 mice per group). (C) Left ventricular ejection fractions assessed at seven or 14 days after initiation of treatment with either CP-673451 or vehicle control as measured by cardiac MRI (n=5 mice per group). (D) Coronary flow reserve assessed at seven or 14 days after initiation of treatment with CP-673451 or vehicle (n=5 mice per group). (E) Confocal micrographs from representative cardiac sections showing staining for CD31 (red), NG2 (green), and the merged image (bottom left) from mice treated with vehicle control (top panels) or CP-673451 for 14 days. Scale bar = 20 μm. (F) Western blot probed for NG2 and phospho-/total levels of PDGFR-β from hearts of mice treated with vehicle for seven days or with CP-673451 for three or seven days. Concentrations of PDGFR-β (G) or NG2 (H) in cardiac lysates from mice treated with CP-673451 for three or seven days relative to levels in control-treated mice, as measured by quantitative densitometry. Values are normalized to levels of GAPDH (n=4 independent samples per group). * $p < 0.05$

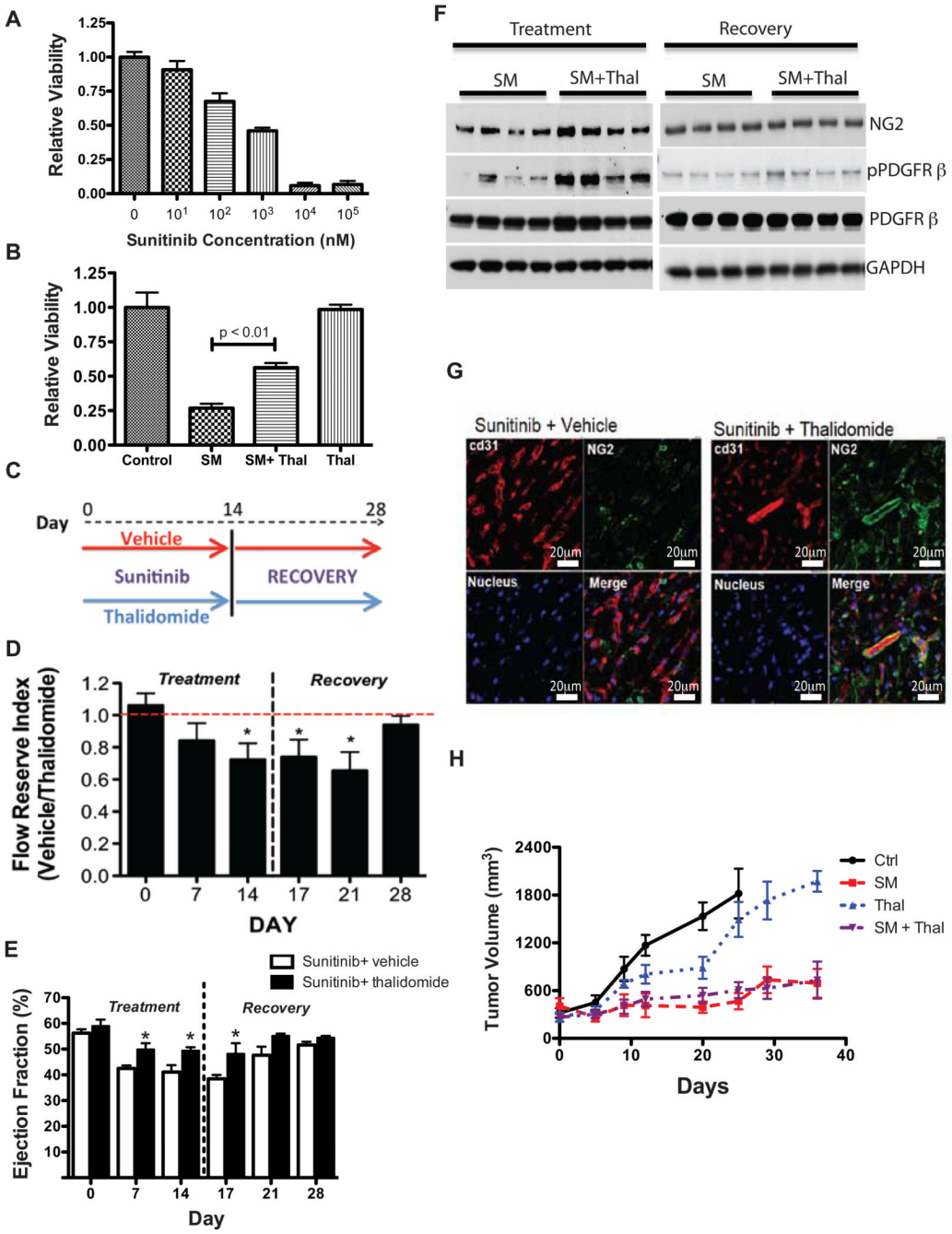

Fig. 6. Sunitinib-induced pericyte cytotoxicity is ameliorated by co-treatment with thalidomide

(B) Pericyte viability measured by MTT assay after incubation for 24 hours with sunitinib at the indicated dosages. 0 nM sunitinib cells were treated with DMSO only, and data are presented as MTT values relative to 0 nM sunitinib cell values. (B) Pericyte viability measured by MTT assay after 24 hours of treatment with DMSO (control), sunitinib malate (SM, 1 μM), thalidomide (Thal, 1 μM) plus sunitinib (SM + Thal) or thalidomide alone (Thal). Data presented as MTT values relative to control. (C) Overview of the protocol for *in vivo* thalidomide rescue experiments. (D) Coronary flow reserve in sunitinib-treated mice co-treated with either vehicle or thalidomide for 14 days followed by a 14-day recovery period (n=5–8 mice per group per time point). Data are shown as coronary flow reserve

index, the ratio of coronary flow reserve in mice treated with sunitinib plus vehicle to coronary flow reserve in mice treated with sunitinib plus thalidomide (denoted “vehicle/thalidomide”). (E) Left ventricular ejection fraction in sunitinib-treated mice co-treated with either vehicle or thalidomide for 14 days followed by a 14-day recovery period. (F) Western blot of cardiac lysates from mice co-treated with sunitinib plus vehicle or thalidomide after 14 days of treatment (left) or after recovery for 14 days, probed for NG2 and phospho-/total PDGFR-β. (G) Confocal micrographs from representative cardiac sections showing staining for CD31 (red), NG2 (green), DAPI (bottom left) and the merged image (bottom right) from mice treated with sunitinib + vehicle (left panels) or sunitinib + thalidomide (right panels) for 14 days. Scale bar = 20 μm. (H) Average tumor volume over time in vehicle, thalidomide, sunitinib or sunitinib + thalidomide treated mice (n=6–10 mice per group). All results presented in this figure are representative of 2–4 independent experiments, * $p < 0.05$.